第 34 卷第 4 期
2018 年 4 月

无 机 化 学 学 报
CHINESE JOURNAL OF INORGANIC CHEMISTRY

Vol.34 No.4
757-766

基于吡嗪–吡啶–酰腙配体的三个配合物的制备及其荧光和光催化性能

徐周庆[1] 何亚玲[1] 李晴晴[1] 张培玲*,[2] 李慧军*,[1] 王 元*,[1]

([1]河南理工大学化学化工学院,焦作 454000)

([2]河南理工大学物理与电子信息学院,焦作 454000)

摘要:合成了 3 个配合物{[$Zn_3(L)_2(SO_4)_2(H_2O)_4$]·$H_2O$}$_n$ (**1**)、{[$Cd_2(L)_2(SO_4)(H_2O)$]·H_2O}$_n$ (**2**)和{[Cd(L)I]·CH_3OH}$_n$ (**3**)(HL=*N*′-nicotinoylpyrazine-2-carbohydrazonamide),并通过单晶 X 射线衍射、红外、元素分析和粉末 X 射线衍射等手段进行表征。配合物 **1** 中,采用 μ_3-$\eta^1\eta^1\eta^1$ 配位模式的 SO_4^{2-} 把 Zn(Ⅱ)连接成无机网状二维平面(*bc* 面),有机配体 HL 交错的分布在网状平面的两侧,这些二维层在分子间氢键的作用下形成三维超分子结构。配合物 **2** 是由配体 HL 连接[$(Cd2)_2(\mu_2$-$SO_4)_2$]和 Cd1 两种节点形成的二维结构,相邻的二维层在 $\pi\cdots\pi$ 堆积作用下形成三维超分子结构。配合物 **3** 是一维的 Z 字链结构,这些一维链在氢键的连接作用下形成二维的超分子网络结构。光催化降解亚甲基蓝实验结果表明,在双氧水存在时配合物 **1**~**3** 均表现出很好的降解效果。

关键词:金属–有机框架;荧光;光催化降解

中图分类号:O614.24$^+$1;O614.24$^+$2 **文献标识码**:A **文章编号**:1001-4861(2018)00-0000-10

DOI:10.11862/CJIC.2018.104

Three Complexes Based on Pyridine-Pyrazine-Hydrazone Ligand: Syntheses, Photocatalysis and Luminescent Properties

XU Zhou-Qing[1] HE Ya-Ling[1] LI Qing-Qing[1] ZHANG Pei-Ling*,[2] LI Hui-Jun*,[1] WANG Yuan*,[1]

([1]*College of Chemistry and Chemical Engineering, Henan Polytechnic University, Jiaozuo, Henan* 454000, *China*)

([2]*College of Physics and Electronic Information, Henan Polytechnic University, Jiaozuo, Henan* 454000, *China*)

Abstract: Three novel complexes, namely {[$Zn_3(L)_2(SO_4)_2(H_2O)_4$]·$H_2O$}$_n$ (**1**), {[$Cd_2(L)_2(SO_4)(H_2O)$]·H_2O}$_n$ (**2**) and {[Cd(L)I]·CH_3OH}$_n$ (**3**). (HL=*N*′-nicotinoylpyrazine-2-carbohydrazonamide), have been synthesized and characterized by elemental analyses, infrared spectra and single-crystal X-ray diffraction analyze. In complex **1**, Zn(Ⅱ) ions are connected by μ_3,$\eta^1\eta^1\eta^1$-SO_4^{2-} anions to form a inorganic layer motif in *bc* plane, and the L^- ligands are decorated on both sides of the layer. Adjacent layers are connected by hydrogen-bonding interactions giving rise to 3D supramolecular network. The 2D complex **2** is formed by the [$(Cd2)_2(\mu_2$-$SO_4)_2$] units and Cd1 ions which are connected by the ligands. Adjacent layers of **2** are extended into 3D supramolecular network by $\pi\cdots\pi$ interactions. Zigzag 1D chains of complex **3** are connected by intermolecular hydrogen bonds into extended plane structure. The photocatalytic degradation of methylene blue (MB) results indicate that complexes **1**~**3** are excellent candidates as photocatalysts in decomposing MB with the presence of H_2O_2. In addition, the luminescent properties of these three complexes have been studied in the solid state. CCDC: 1544978, **1**; 1544980, **2**; 1544979, **3**.

Keywords: metal-organic framework; luminescent property; photocatalytic degradation

收稿日期:2017-09-17。收修改稿日期:2018-01-24。

国家自然科学基金(No.21601050),NSFC-河南地区联合基金(No.U1604124),河南省科技攻关项目(No.152102210314),河南省高等学校重点科研项目(No.16A150010),河南理工大学青年骨干教师项目(No.672105/198)和河南理工大学博士基金(No.72103/001/103)资助。

*通信联系人。E-mail:plzhang@hpu.edu.cn,lihuijunxgy@hpu.edu.cn,wangyuan08@hpu.edu.cn;会员登记号:S06N4036M111。

In view of the pursuing "green life", degradation of organic dyes has been given tremendous attention[1-2]. In this regard, removing the poor biodegradable dyes from water has been attracting a great deal of attention and becoming a hot research topic[3-4]. There have been considerable efforts in treating wastewater based on adsorption and separation[5-6], chemical treatment[7], and photocatalytic methods[8]. Among these, photocatalysis offers a convenient and recyclable approach and has been applied in ecologically eliminating organic dyes and other noxious contaminants[9]. Therefore, the construction of inexpensive, stable, and efficient materials with improved photocatalytic properties is extremely urgent.

Recently, some results have demonstrated that metal-organic coordination polymers (MOCPs) are efficient photocatalysts on the degradation of organic dyes, water splitting, or photoreduction of CO_2 [10-11]. How to form efficient, stable, photocatalytic MOCPs is still a big challenge. Because the ligand plays an important role in the construction of functional MOCPs, the rational design of organic ligand is the vital factor in the formation of the targeted MOCPs. Hydrazone, a kind of Schiff base ligand, have been attracting much attention because of their strong tendency to chelate to transition metals[12-13]. Especially, the hydrazone asymmetrically decorated by different aza-aromatics possessing tridentate chelating and bridging coordinating sites may be a good cand-idate to construct novel MOCPs with unique structure characters and interesting properties[14-15].

In view of these points, we employed *N*′-nicotinoylpyrazine-2-carbohydrazonamide (HL) as ligand to achieve three novel complexes: $\{[Zn_3(L)_2(SO_4)_2(H_2O)_4]\cdot H_2O\}_n$ (**1**), $\{[Cd_2(L)_2(SO_4)(H_2O)]\cdot H_2O\}_n$ (**2**) and $\{[Cd(L)I]\cdot CH_3OH\}_n$ (**3**). The photocatalytic research result indicates that complexes **1**~**3** are good candidates as photocatalysts in decomposing MB with the presence of H_2O_2. In addition, the luminescent properties of these three complexes have been studied in the solid state.

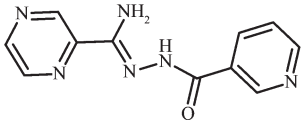

Scheme 1 Structure of HL

1 Experimental

1.1 Materials and measurement

All chemicals were commercially purchased except for HL which was synthesized according to the literature[15]. Elemental analyses for carbon, hydrogen and nitrogen were performed on a Thermo Science Flash 2000 element analyzer. FT-IR spectra were obtained in KBr disks on a PerkinElmer Spectrum One FTIR spectrophotometer in 4 000~450 cm^{-1} spectral range. Diffuse reflectance data were collected using a Shimadzu UV-3600 spectrophotometer, and the Kubelka-Munk function was used to estimate the optical band gap. The powder X-ray diffraction (PXRD) studies were performed with a Bruker AXS D8 Discover instrument (Cu $K\alpha$ radiation, λ=0.154 184 nm, U=40 kV, I=40 mA) over the 2θ range of 5°~50° at room temperature. The photoluminescent properties were measured on an F-4500 FL Spectrophotometer.

1.2 Preparations of the complexes 1~3

$\{[Zn_3(L)_2(SO_4)_2(H_2O)_4]\cdot H_2O\}_n$ (**1**). A mixture of HL (0.05 mmol, 12.1 mg), $ZnSO_4\cdot 7H_2O$ (0.10 mmol, 28.7 mg), absolute methyl alcohol (3 mL), H_2O (3 mL) and *N*,*N*-dimethylacetamide (DMA) (2 mL) was placed in a Teflon-lined stainless steel vessel (20 mL), heated to 80 ℃ for 3 days, and then cooled to room temperature at a rate of 5 ℃·h^{-1}. Yellow block crystals of **1** were obtained and picked out, washed with distilled water and dried in air. Yield: 18.4 mg, 74.2% (based on HL). Elemental analysis: Calcd. for $C_{22}H_{22}N_{12}O_{13}S_2Zn_3$(%): C 28.63, H 2.40, N 18.21; Found (%): C 26.65, H 2.38, N 18.26. IR (KBr, cm^{-1}): 3 455, 1 636, 1 528, 1 497, 1 451 1 410, 1 141, 1 012.

$\{[Cd_2(L)_2(SO_4)(H_2O)]\cdot H_2O\}_n$ (**2**). A mixture of HL (0.05 mmol, 7.4 mg), $CdSO_4\cdot 8/3H_2O$ (12.815 mg, 0.1 mmol), absolute ethanol (2 mL) and H_2O (6 mL) was placed in a sealed flask (20 mL), heated to 80 ℃ for 3 days. White block crystals of **2** were obtained and picked out, washed with distilled water and dried in air. Yield: 14.9 mg, 71.0% (based on HL). Elemental analysis: Calcd. for $C_{22}H_{22}Cd_2N_{12}O_8S$(%): C 31.48, H

2.64, N 20.02; Found (%): C 31.51, H 2.68, N 20.08. IR (KBr, cm^{-1}): 3 453, 1 657, 1 528, 1 476, 1 394, 1 130, 1 053, 981.

$\{[Cd(L)I]\cdot CH_3OH\}_n$ (**3**). A mixture of HL (0.05 mmol, 7.4 mg), CdI_2(18.3 mg, 0.1 mmol), distilled H_2O (4 mL), methyl alcohol (4 mL) and *N*,*N*-dimethylacetamide (DMA) (2 mL) were sealed in a 20 mL little bottle and heated at 80 ℃ for 3 days. After the mixture was cooled to room temperature, yellow block crystals of **3** were obtained and picked out, washed with distilled water and dried in air. Yield: 8.71 mg, 68.1% (based on HL). Elemental analysis: Calcd. for $C_{12}H_{13}CdIN_6O_2$(%): C 28.12, H 2.56, N 16.39; Found(%): C 28.16, H 2.48, N 16.42. IR (KBr, cm^{-1}): 3 458, 1 654, 1 531, 1 469, 1 391, 1 138, 1 048, 1 008.

1.3 X-ray crystallography

X-ray Single-crystal diffraction analysis of **1**~**3** was carried out on a Bruker SMART APEX Ⅱ CCD diffractometer equipped with a graphite monochromated Mo $K\alpha$ radiation (λ=0.071 073 nm) by using φ-ω scan technique at room temperature. The structures were solved via direct methods (SHELXS-97)[16], and refined by the full-matrix least-squares method on F^2 with anisotropic thermal parameters for all non-H atoms (SHELXL-97). The empirical absorption corrections were applied by the SADABS program[17]. The H-atoms of carbon were assigned with common isotropic displacement factors and included in the final refinement by the use of geometrical restraints. H-atoms of water molecules were first located by the Fourier maps and then refined by the riding mode. The crystallographic data for complexes **1**~**3** are listed in Table 1. Moreover, the selected bond lengths and bond angles are listed in Table 2.

CCDC: 1544978, **1**; 1544980, **2**; 1544979, **3**.

Table 1　Crystal data and structural refinement of complexes 1~3

Complex	1	2	3
Empirical formula	$C_{22}H_{22}N_{12}O_{13}S_2Zn_3$	$C_{22}H_{22}Cd_2N_{12}O_8S$	$C_{12}H_{13}CdIN_6O_2$
Formula weight	922.75	839.38	512.58
Temperature / K	296	296	296
Crystal system	Orthorhombic	Triclinic	Monoclinic
Space group	*Aba*2	$P\bar{1}$	$P2_1/c$
a / nm	1.678 1(2)	1.053 6(3)	1.229 7(6)
b / nm	1.965 4(2)	1.144 9(4)	1.000 2(5)
c / nm	0.925 53(11)	1.190 8(4)	1.307 3(6)
α / (°)		94.754(5)	
β / (°)		95.078(6)	94.593(9)
γ / (°)		97.687(6)	
Volume / nm^3	3.052 6(6)	1.411 5(8)	1.602 7(14)
Z	4	2	4
D_c / ($g\cdot cm^{-3}$)	2.008	1.975	2.124
Absorption coefficient / mm^{-1}	2.564	1.651	3.304
F(000)	1 856	828	976
Crystal size / mm	0.3×0.2×0.1	0.1×0.1×0.08	0.2×0.2×0.08
R_{int}	0.041 9	0.050 4	0.033 0
Reflection collected, unique	7 547, 2 678	638, 4 909	7 888, 2 817
Goodness-of-fit on F^2	0.985	0.986	0.998

Table 2　Selected bond lengths (nm) and angles (°) for complexes 1~3

Complex **1**					
Zn(1)-O(4)^{i}	0.198 4(3)	Zn(1)-N(1)	0.225 9(3)	Zn(2)-O(6)	0.212 8(3)
Zn(1)-N(4)	0.200 2(3)	Zn(2)-N(6)	0.209 4(3)	Zn(2)-O(3)^{iii}	0.217 5(3)

Continued Table 2

Zn(1)-O(2)	0.202 3(3)	Zn(2)-N(6)^{ii}	0.209 4(3)	Zn(2)-O(3)^{iv}	0.217 5(3)
Zn(1)-O(1)	0.211 5(3)	Zn(2)-O(6)^{ii}	0.212 8(3)		
O(4)^{i}-Zn(1)-N(4)	125.28(13)	O(4)^{i}-Zn(1)-O(2)	91.52(12)	O(1)-Zn(1)-N(1)	149.93(11)
N(6)^{ii}-Zn(2)-O(3)^{iii}	95.68(11)	N(4)-Zn(1)-O(2)	142.88(13)	N(6)-Zn(2)-N(6)^{ii}	95.76(19)
O(6)^{ii}-Zn(2)-O(3)^{iii}	89.08(11)	O(4)^{i}-Zn(1)-O(1)	101.14(12)	N(6)-Zn(2)-O(6)^{ii}	176.08(14)
O(6)-Zn(2)-O(3)^{iii}	85.37(11)	N(4)-Zn(1)-O(1)	76.19(11)	N(6)ii-Zn(2)-O(6)^{ii}	88.01(12)
N(6)-Zn(2)-O(3)^{iv}	95.68(11)	O(2)-Zn(1)-O(1)	103.71(12)	N(6)-Zn(2)-O(6)	88.01(12)
N(6)^{ii}-Zn(2)-O(3)^{iv}	89.51(11)	O(4)^{i}-Zn(1)-N(1)	99.67(12)	N(6)^{ii}-Zn(2)-O(6)	176.08(14)
O(6)^{ii}-Zn(2)-O(3)^{iv}	85.37(11)	N(4)-Zn(1)-N(1)	74.10(12)	O(6)^{ii}-Zn(2)-O(6)	88.23(17)
O(6)-Zn(2)-O(3)^{iv}	89.08(11)	O(2)-Zn(1)-N(1)	97.16(13)	N(6)-Zn(2)-O(3)^{iii}	89.51(11)
O(3)^{iii}-Zn(2)-O(3)^{iv}	172.26(17)				
Complex **2**					
Cd(1)-N(4)	0.221 7(8)	Cd(1)-N(7)	0.250 8(8)	Cd(2)-O(7)	0.230 8(7)
Cd(1)-N(10)	0.222 1(8)	Cd(1)-N(1)	0.254 1(7)	Cd(2)-N(2)^{ii}	0.235 8(7)
Cd(1)-O(1)	0.223 6(6)	Cd(2)-O(3)^{i}	0.228 3(6)	Cd(2)-N(12)^{iii}	0.236 7(8)
Cd(1)-O(2)	0.230 9(7)	Cd(2)-N(6)	0.230 1(8)	Cd(2)-O(3)	0.243 8(6)
N(4)-Cd(1)-N(10)	151.6(3)	N(4)-Cd(1)-N(1)	67.3(2)	O(7)-Cd(2)-N(2)^{ii}	84.7(3)
N(4)-Cd(1)-O(1)	71.6(2)	N(10)-Cd(1)-N(1)	84.3(3)	O(3)^{i}-Cd(2)-N(12)^{iii}	113.5(2)
N(10)-Cd(1)-O(1)	136.4(3)	O(1)-Cd(1)-N(1)	138.1(2)	N(6)-Cd(2)-N(12)^{iii}	90.4(3)
N(4)-Cd(1)-O(2)	109.5(2)	O(2)-Cd(1)-N(1)	92.0(3)	O(7)-Cd(2)-N(12)^{iii}	86.3(3)
N(10)-Cd(1)-O(2)	69.5(3)	N(7)-Cd(1)-N(1)	83.9(3)	N(2)^{ii}-Cd(2)-N(12)^{iii}	96.1(3)
O(1)-Cd(1)-O(2)	109.5(2)	O(3)^{i}-Cd(2)-N(6)	94.1(3)	O(3)i-Cd(2)-O(3)	75.2(2)
N(4)-Cd(1)-N(7)	106.9(3)	O(3)^{i}-Cd(2)-O(7)	159.5(2)	N(6)-Cd(2)-O(3)	88.9(2)
N(10)-Cd(1)-N(7)	68.8(3)	N(6)-Cd(2)-O(7)	91.1(3)	O(7)-Cd(2)-O(3)	85.1(2)
O(1)-Cd(1)-N(7)	100.5(3)	O(3)^{i}-Cd(2)-N(2)^{ii}	87.7(3)	N(2)^{ii}-Cd(2)-O(3)	83.9(2)
O(2)-Cd(1)-N(7)	138.3(2)	N(6)-Cd(2)-N(2)^{ii}	171.9(3)	N(12)^{iii}-Cd(2)-O(3)	171.4(3)
Complex **3**					
Cd(1)-N(4)	0.222 2(5)	Cd(1)-N(6)^{i}	0.229 6(5)	Cd(1)-O(1)	0.232 5(4)
Cd(1)-N(1)	0.251 5(6)	Cd(1)-I(1)	0.269 54(13)		
N(4)-Cd(1)-N(6)^{i}	104.02(17)	N(4)-Cd(1)-O(1)	70.76(15)	N(6)^{i}-Cd(1)-N(1)	89.73(18)
N(6)^{i}-Cd(1)-I(1)	104.52(12)	N(6)^{i}-Cd(1)-O(1)	101.34(16)	O(1)-Cd(1)-N(1)	138.80(15)
O(1)-Cd(1)-I(1)	114.27(10)	N(4)-Cd(1)-N(1)	68.06(17)	N(4)-Cd(1)-I(1)	149.17(12)
N(1)-Cd(1)-I(1)	100.67(13)				

Symmetry codes: ^{i} $-x+2, -y+3/2, z+1/2$, ^{ii} $-x+2, -y+2, z$, ^{iii} $-x+2, -y+2, z+1$ for **1**; ^{i} $-x+2, -y+2, -z+2$, ^{ii} $x+1, y+1, z$, ^{iii} $x+1, y, z$ for **2**; ^{i} $-x+1, y+1/2, -z+3/2$ for **3**.

1.4 Photocatalytic experiments

To evaluate the photocatalytic activities of these three complexes, the photocatalytic degradation of methylene blue (MB) aqueous solution was performed at ambient temperature[18]. The procedure was as follows: 20 mg of the desolvated samples was dispersed into 100 mL of MB aqueous solution (12.75 mg·L^{-1}), followed by the addition of four drops of hydrogen peroxide solution (H_2O_2, 30%). The suspensions were magnetically stirred in the dark for over 1 h to ensure adsorption equilibrium of MB onto the surface of samples. A 300 W xenon arc lamp was used as a light source to irradiate the above solutions for 0, 20, 40, 60, 80, and 100 min. And the corresponding reaction

solutions were filtered and the absorbance of MB aqueous solutions was then measured by a spectrophotometer. For comparison, the contrast experiment was completed under the same conditions without any catalyst. The characteristic peak (λ=664 nm) for MB was employed to monitor the photocatalytic degradation process.

2 Results and discussion

2.1 Crystal structures of complexes 1~3

Single-crystal X-ray crystallographic analysis reveals that complex **1** crystallizes in the orthorhombic space group *Aba*2. The asymmetric unit of **1** consists of one and a half Zn(Ⅱ) ions, one L^- ligand, one SO_4^{2-} anion and half lattice water molecule. The HL ligand indeed coordinate to two Zn(Ⅱ) ions by the tridentate chelating site and the bridging pyridine nitrogen atom. As shown in Fig.1a, the Zn1 ion is coordinated by two N atoms and one carbonyl oxygen atom from one L^- ligand, two oxygen atoms from two SO_4^{2-} anions, thus creating distorted trigonal bipyramid coordination geometry. The Zn2 ion adopts a slightly distorted octahedral geometry coordinated to two N atoms from two L^- ligands, two oxygen atoms from two SO_4^{2-} anions and two coordinated water molecules. The Zn-O bond distances are in the range of 0.198 4(3) to 0.217 5(3) nm, and the Zn-N bond length is in the range of 0.200 2(4)~0.225 9(3) nm. The SO_4^{2-} anion in **1** connects three Zn(Ⅱ) ions adopting a $\mu_3,\eta^1\eta^1\eta^1$-coordination mode. In this way, Zn(Ⅱ) ions are connected by SO_4^{2-} anions to form the inorganic layer motif in *bc* plane (Fig.1b). The L^- ligands are decorated on both sides of the layer motif by the tridentate chelating site and the bridging pyridine nitrogen atom (Fig.1c). Moreover, the SO_4^{2-} anions and the lattice O7 water molecules join adjacent layers through the hydrogen-bonding interactions (N3⋯O5^{iii} 0.301 3(5) nm, ∠N3-H3A-O5^{iii}=158.3°, O6⋯O7^{iv} 0.278 3(5) nm, ∠O6-H6A⋯O7^{iv}=168.8°, and O6⋯O5^{ii} 0.269 5(4) nm, ∠O6-H6B⋯O5^{ii}=150.5°) giving rise to 3D

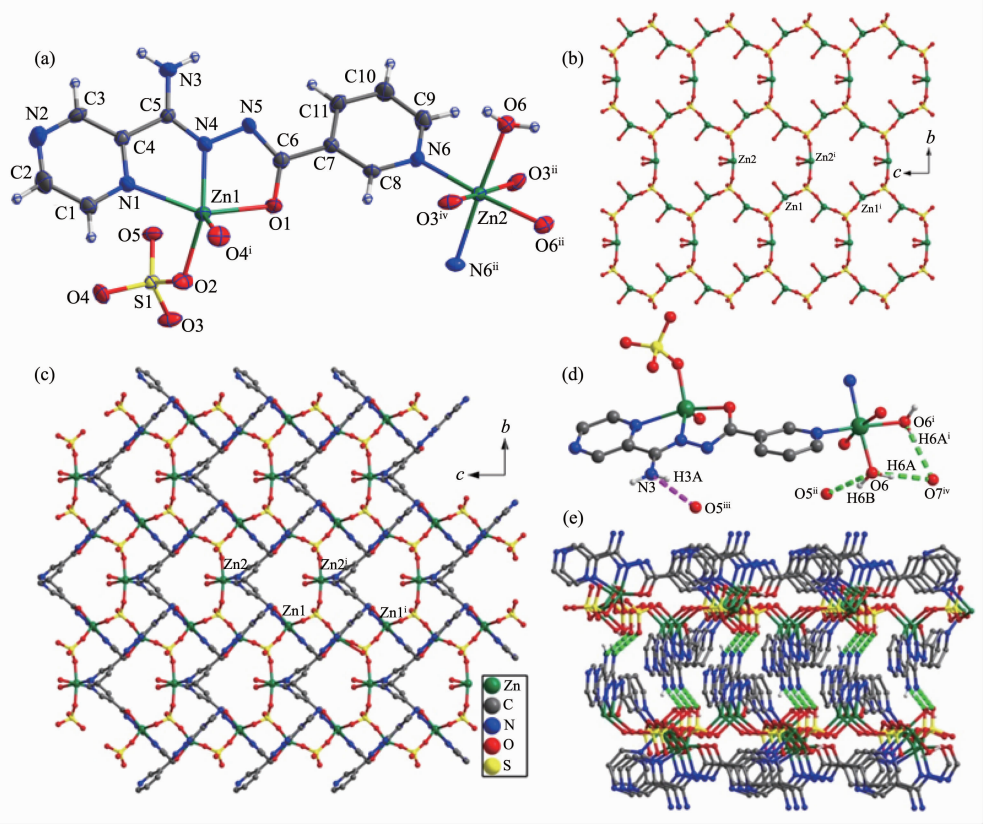

Symmetry codes: [i] 1+*x*, 1+*y*, *z*; [ii] 1+*x*, *y*, *z*; [iii] 2−*x*, 2−*y*, 2−*z*; [iv] −1+*x*, *y*, *z*

Fig.1 Crystal structure of complex **1**: (a) coordination environment of center ions; (b) inorganic layer motif; (c) 2D plane structure; (d) hydrogen bonds; (e) 3D supramolecular network connected by π-π stacking

supramolecular network (Fig.1d and 1e).

X-ray single crystal structure analysis reveals that **2** crystallizes in the triclinic space group $P\bar{1}$. The asymmetric unit of crystal **2** consists of two six-coordinated Cd(Ⅱ) ions, two L^- ligands, one SO_4^{2-} anion, one coordinated water molecule and one lattice water molecule. As shown in Fig.2a, the six-coordinated Cd1 ion is surrounded by two L^- ligands through the tridentate chelating sites (Cd-N 0.221 7(8) ~0.254 1(7) nm, Cd-O 0.223 6(6)~0.230 9(7) nm), and the Cd2 is coordinated to three N atoms from three L^- ligands, two oxygen atoms from two SO_4^{2-} anions and one coordinated water molecule (Cd-N 0.230 1(8)~0.236 7(8) nm, Cd-O 0.228 3(6)~0.243 8(6) nm). As shown in Fig.2b, one $[(Cd2)_2(\mu_2\text{-}SO_4)_2]$ unit joins adjacent six Cd1 by six L^- ligands and each Cd1 connects three $[(Cd2)_2(\mu_2\text{-}SO_4)_2]$ units to form a layer motif (Fig. 2c). Furthermore, the N7-containing pyrazine rings and N12-containing pyridyl rings in adjacent layer motifs are nearly parallel to each other, which can provide the chance for the formation of $\pi\cdots\pi$ interactions with the C-to-centroid distance being 0.352 7(2) and 0.373 0(5) nm. All these $\pi\cdots\pi$ interactions extend adjacent layers into 3D supramolecular network as shown in Fig.2d.

Single-crystal X-ray crystallographic analysis reveals that complex **3** crystallizes in the monoclinic space group $P2_1/c$ and its asymmetric unit consists of one Cd(Ⅱ) ion, one L^- ligand, one I^- anion and one lattice methyl alcohol molecule. The Cd(Ⅱ) ion is coordinated by two N atoms and one oxygen atom of one ligand, one N atom from another ligand and one iodide anion resulting in a distorted quadrangular pyramid geometry. The measured Cd-O distance is 0.225(4) nm, Cd-N distance is in the range of 0.222 2(5)~0.251 5(6) nm, and Cd-I distance is 0.269 54(13) nm, respectively. The bond angle around the Cd(Ⅱ) center lies in the range of 68.06(17)°~149.17(12)°. The HL ligand coordinates to two Cd(Ⅱ) ions by the tridentate chelating site and the bridging pyridine nitrogen atom, which give rise to the formation of the zigzag 1D chain (Fig.3b). Furthermore, the zigzag 1D chain are connected by the intermolecular hydrogen bonds N3–H3B···O1^{ii}, N3–H3A···O2 and the O2–H2A···O1^{i} into

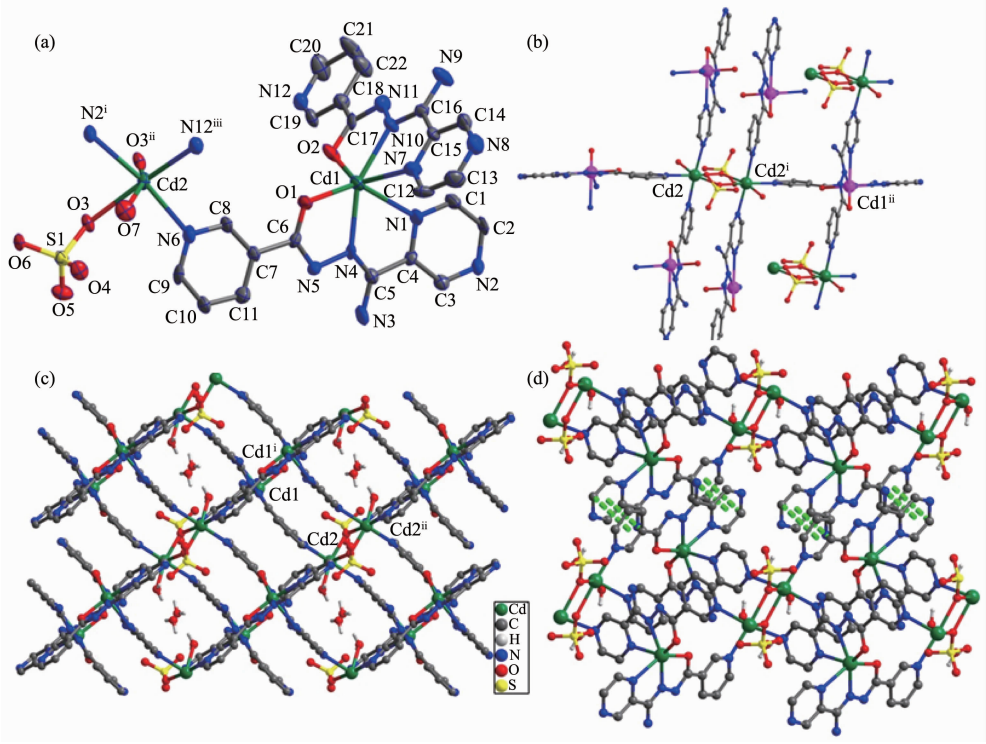

Symmetry codes: ^{i} 1+x, 1+y, z; ^{ii} 1+x, y, z; ^{iii} 2–x, 2–y, 2–z

Fig.2 Crystal structure of complex **2**: (a) ORTEP drawing of **2** with 30% thermal ellipsoids; (b) connection mode of mononuclear and dinuclear unit; (c) 2D structure; (d) 3D supramolecular architecture connected by π-π stacking

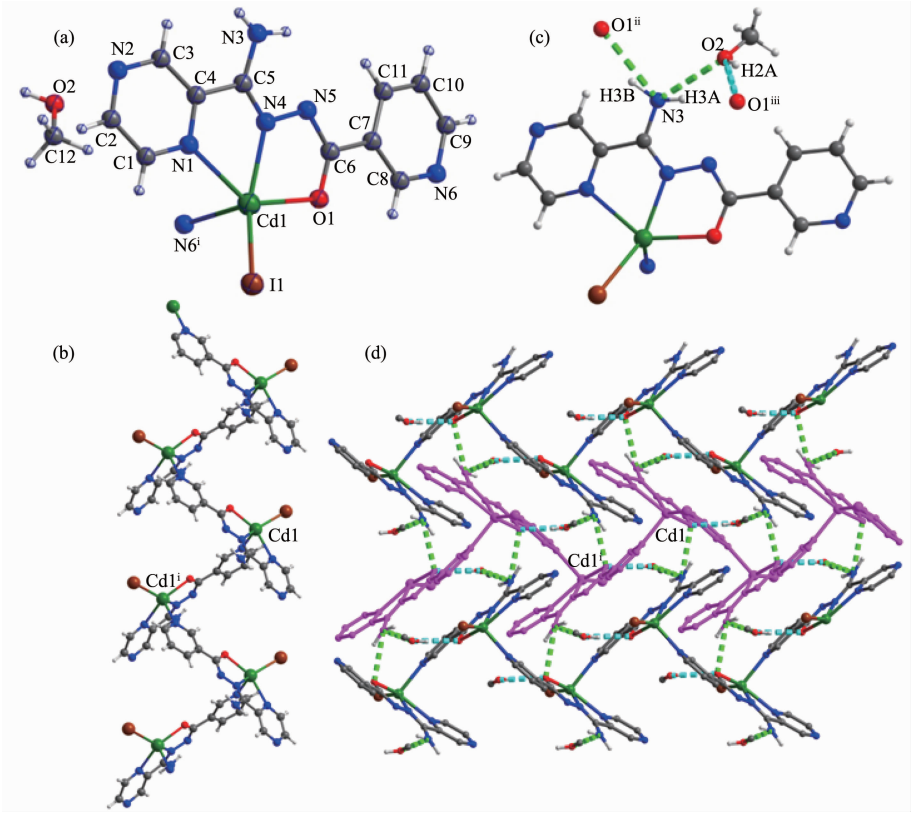

Symmetry codes: [i] $-x+1, y-1/2, -z+3/2$; [ii] $x, -y+1/2, z-1/2$; [iii] $x, y+1, z$

Fig.3　Crystal structure of complex **3**: (a) ORTEP drawing of **3** with 30% thermal ellipsoids; (b) zigzag 1D chain; (c) hydrogen bonds interaction; (d) 2D supramolecular architecture connected by hydrogen bonds

extended plane structure (Fig.3c and 3d).

2.2　PXRD patterns and photoluminescent properties

In order to evaluate the phase purity of **1**~**3**, powder X-ray diffraction experiments have been performed at room temperature (Fig.4). Their high purity solid state phases were confirmed by the good match of the patterns for the as-synthesized samples and simulated ones from the single-crystal data.

Luminescent properties of MOCPs based on d^{10} metal ions are of special interest due to their prospective applications in electroluminescent displays, nonlinear optical (NLO) devices and so on[19]. The combination of organic linkers and metal centers in MOCPs provides an efficient route to a new type of photoluminescent materials with potential applications because of their structure- and metal-dependent emission. In this context, solid-state photoluminescent behavior of HL as well as complexes **1**~**3** are examined in the solid state at room temperature.

As shown in Fig.4d, the HL ligand are nearly non-fluorescent in the range of 400 ~650 nm for excitation wavelength of 370 nm at ambient temperature[20]. The intense emissions occur at 450 and 490 nm for complexes **1** and **2** with the excitation wavelength of 370 nm. The emissions are neither metal-to-ligand charge transfer (MLCT) nor ligand-to-metal transfer (LMCT) in nature since Zn(Ⅱ) is difficult to oxidize or reduce due to its d^{10} configuration[21]. Thus, they may be assigned to intraligand ($\pi^*\rightarrow n$ or $\pi^*\rightarrow\pi$) emission. The enhancement of luminescence in d^{10} complexes may be attributed to ligand chelation to the metal center, which effectively increases the rigidity of the ligand and reduces the loss of energy by radiationless decay[22]. In comparison, complex **3** shows relatively weak emission bands. This significantly weakened intensity of the emission is probably attributed to the quenching effect of iodide ions[23]. The observation indicates that the complexes of **1** and **2** may be candidates for potential photoactive materials.

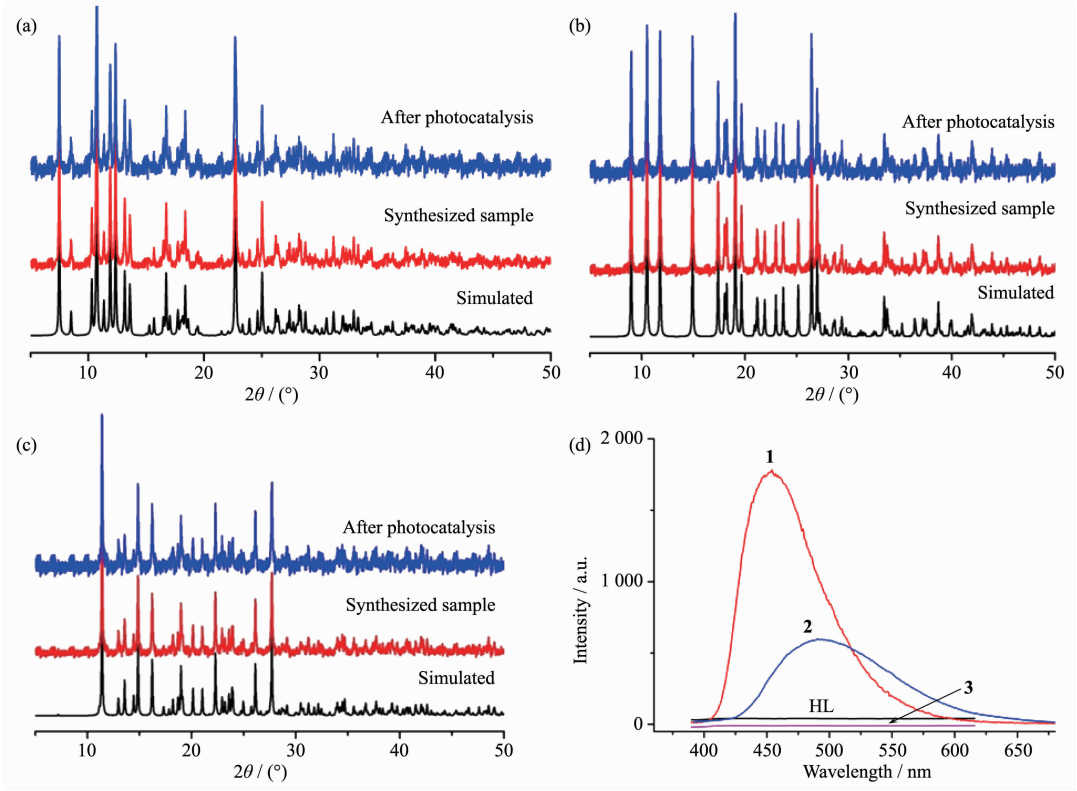

Fig.4 PXRD patterns of complex **1** (a), **2** (b), **3** (c) and emission spectra of the ligand and complexes **1~3** at room temperature (d)

The fluorescence property means the transition from the excited state to the ground state at the same energy level. While the photocatalytic property requires the excited electrons stay at the surface of the material long enough to participate surface oxidation-reduction reaction. Therefore, the fluorescence properties and photocatalytic properties are theoretically reverse process. In general, materials with good photocatalytic performance will not be too strong fluorescence. By the above points, the photocatalytic properties of complexes **1~3** need to be investigated.

2.3 Photocatalysis property

The band gap of complexes **1~3** was measured by a solid state ultraviolet-visible (UV-Vis) diffuse reflectance measurement method at room temperature. In a plot of K-M function versus energy, the band gap E_g is defined as the intersection point among the energy axis and line extrapolated of the linear portion[24]. The K-M function, $F=(1-R)^2/(2R)$ (R is the reflectance of an infinitely thick layer at a given wavelength), can be converted from measured diffuse reflectance data. As shown in Fig.5, the E_g values for complexes **1~3** are 2.20, 1.65 and 2.05 eV, respectively. The reflectance spectra show that there exist the optical band gap and semiconductive behaviors in complexes **1~3**, and these complexes can be employed as potential semiconductive materials (the E_g of a semiconductor is 1~3 eV)[25].

In order to evaluate the photocatalytic effectiveness of the complexes **1~3**, the photocatalytic degradation of MB aqueous solution was performed at ambient temperature. As can be seen in Fig.6, the characteristic absorption peak of MB (664 nm) were gradually reduced with time increasing from 0 to 100 min. Besides, the changes in the plot of C_t/C_0 versus irradiation time are shown in Fig.7a to clarify the photocatalytic results (wherein C_t is the concentration at time t of the MB solution and C_0 is the concentration at time t=0 of the MB solution). From Fig.7a, the degradation rate of MB reaches 24% without any photocatalyst, while it increases to 83%, 92% and 85%, respectively, when complexes **1**, **2** and **3** are added to the mixture as catalyst.

The efficiency of the photocatalyst is a function of the balance between charge separation, interfacial

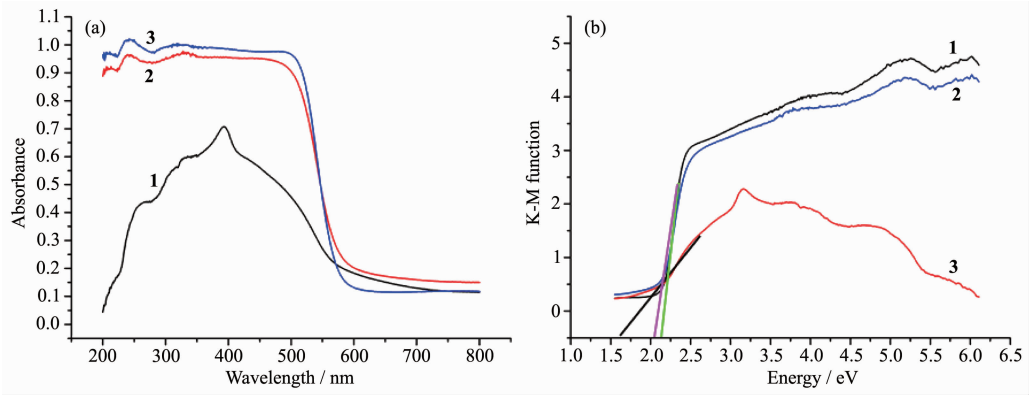

Fig.5　(a) UV-Vis absorption spectra of complexes **1~3**; (b) Kubelka-Munk-transformed diffuse reflectance of complexes **1~3**

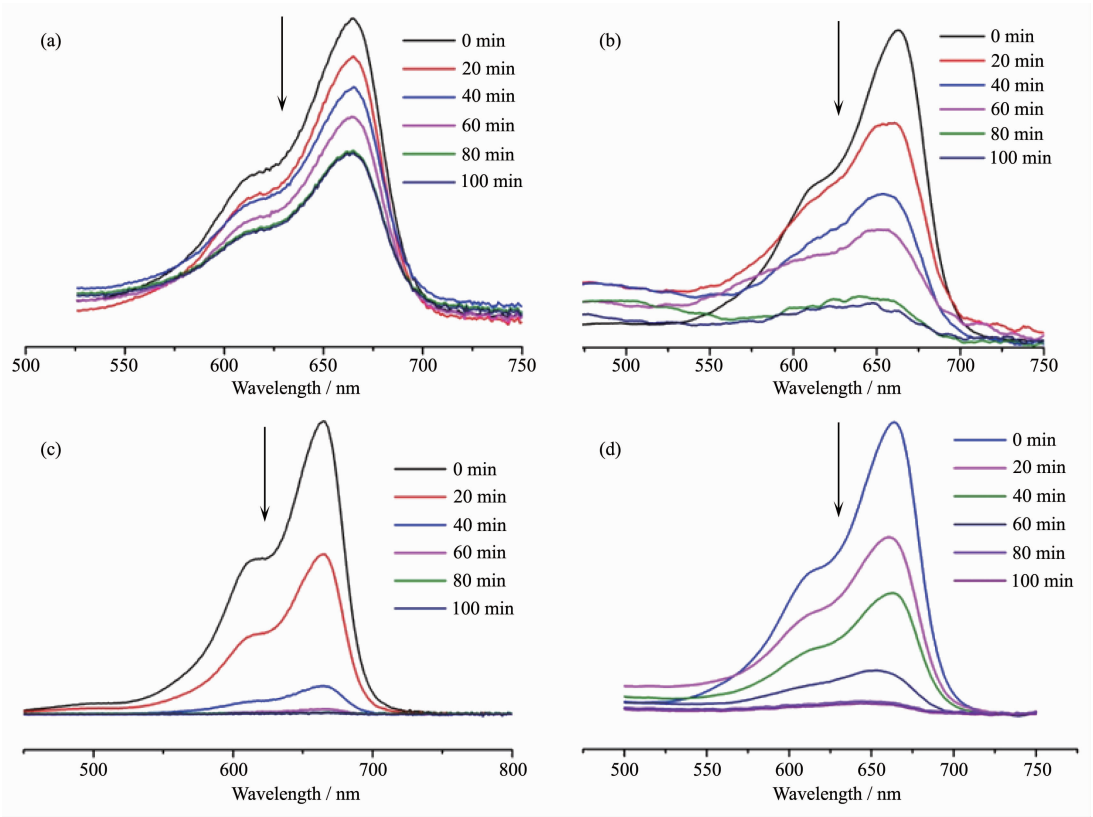

Fig.6　Absorption spectra of the solution of MB without catalyst (a), or with complex **1** (b), **2** (c) and **3** (d) as catalyst, respectively

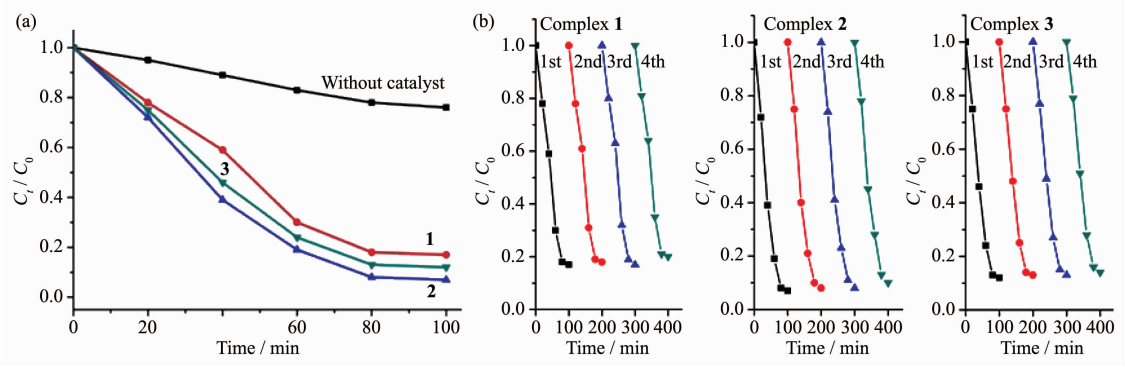

Fig.7　(a) Photodegradation of MB with complexes **1~3**; (b) Recycling experiments using complexes **1~3** for the photocatalytic degradation of MB solution

electron transfer, and charge recombination. In general, a narrow band gap leads to the ease of the charge separation, so the photocatalytic degradation rate of MB should follow the reverse order of band gaps of the complexes. As calculated, the band gaps of complexes **1**~**3** are 2.20, 1.65, and 2.05 eV, respectively. The E_g of **1**~**3** follows the sequence: **2**<**1**≈**3**, and the reverse sequence of band gaps agrees with the degradation rate of MB. In addition, the stabilities of these three complexes are investigated by measuring the powder PXRD patterns after photocatalytic reactions. The PXRD patterns are consistent with those of the original ones, which confirm that these complexes keep their skeleton well after the photocatalytic process. The photocatalytic research result indicates that complexes **1**~**3** are good candidates as photocatalysts in decomposing MB with the presence of H_2O_2 and may have possible application in decomposing other dyestuff.

Further studies about the stability and reproducibility are also carried out (Fig.7b), and the results show that compounds **1**~**3** do not exhibit a significant decrease after four runs in the same photocatalytic tests (83% for **1**, 93% for **2**, and 85% for **3** for the first cycles, 82% for **1**, 92% for **2**, and 85% for **3** for the second cycles, 83% for **1**, 92% for **2**, and 84% for **3** for the third cycles, 80% for **1**, 90% for **2**, and 82% for **3** for the fourth cycles), which manifest that the compounds **1**~**3** as photocatalysts are very stable and possess good reproducibility.

3 Conclusions

In summary, an asymmetric triazolate derivative, *N*′-nicotinoylpyrazine-2-carbohydrazonamide (HL), was employed to achieve three novel MOCPs $\{[Zn_3(L)_2(SO_4)_2(H_2O)_4]\cdot H_2O\}_n$ (**1**), $\{[Cd_2(L)_2(SO_4)(H_2O)]\cdot H_2O\}_n$ (**2**) and $\{[Cd(L)I]\cdot CH_3OH\}_n$ (**3**). The structure of these complexes was characterised by single-crystal X-ray diffraction, powder X-ray diffraction, elemental analyses and infrared spectra. The photocatalytic experiment rusult indicates that complexes **1**~**3** are good candidates as photocatalysts in decomposing MB with the presence of H_2O_2.

References:

[1] Yang H, He X W, Wang F, et al. *J. Mater. Chem.*, **2012**,**22**: 21849-21851

[2] Waranusantigul P, Pokethitiyook P, Kruatrachue M, et al. *Environ. Pollut.*, **2003**,**125**:385-392

[3] Xu X Y, Chen Q C, Yu Y D, et al. *Inorg. Chem.*, **2016**,**55**: 75-82

[4] Herm Z R, Wiers B M, Mason J A, et al. *Science*, **2013**,**340**: 960-964

[5] Lin R B, Chen D, Lin Y Y, et al. *Inorg. Chem.*, **2012**,**51**: 9950-9955

[6] Liu J Q, Wang W J, Luo Z D, et al. *Inorg. Chem.*, **2017**,**56**: 10215-10219

[7] Neupane G P, Tran M D, Yun S J, et al. *ACS Appl. Mater. Interfaces*, **2017**,**9**:11950-11958

[8] Luo L, Lin H S, Li L, et al. *Inorg. Chem.*, **2014**,**53**:3464-3470

[9] Yu X, Fan X, Li Z, et al. *Dalton Trans.*, **2017**,**46**:11898-11904

[10]Jiang D L, Li J, Xing C S, et al. *ACS Appl. Mater. Interfaces*, **2015**,**34**:19234-19242

[11]Lee Y Y, Moon J H, Choi Y S, et al. *J. Phys. Chem. C*, **2017**,**121**:5137-5144

[12]Hussain N, Bhardwaj V K. *Dalton Trans.*, **2016**,**45**:7697-7707

[13]Wang Y N, Yang Q F, Li G H, et al. *Dalton Trans.*, **2014**, **43**:11646-11657

[14]Xu J, Zhou T, Xu Z Q, et al. *J. Mol. Struct.*, **2017**,**1128**:448-454

[15]Xu Z, Mao X, Zhang P, et al. *J. Mol. Struct.*, **2017**,**1128**: 665-673

[16]Sheldrick G M. *SHELXL*97, *Program for the Crystal Structure Refinement*, University of Göttingen, Germany, **1997**.

[17]Sheldrick G M. *SADABS*, University of Göttingen, Germany, **1996**.

[18]Xu C, Rangaiah G P, Zhao X S. *Ind. Eng. Chem. Res.*, **2014**, **53**:14641-14649

[19]Dong Y B, Wang P, Ma J P, et al. *J. Am. Chem. Soc.*, **2007**, **129**:4872-4873

[20]Jin J C, Wang Y Y, Liu P, et al. *Cryst. Growth Des.*, **2010**, **10**:2029-2035

[21]Xiao D R, Li Y G, Wang E B, et al. *Inorg. Chem.*, **2007**,**46**: 4158-4166

[22]Shen S L, Zhao X, Zhang X F, et al. *J. Mater. Chem. B*, **2017**,**5**:289-295

[23]McFadden P D, Frederick K, Argüello L A, et al. *ACS Appl. Mater. Interfaces*, **2017**,**9**:10061-10068

[24]XU Zhou-Qing(徐周庆), HE Ya-Ling(何亚玲), LI Hui-Jun(李慧军), et al. *Chinese J. Inorg. Chem.*(无机化学学报), **2017**,**33**:897-904

[25]LI Hui-Jun(李慧军), YAN Ling-Ling(闫玲玲), WANG Yuan(王元), et al. *Chinese J. Inorg. Chem.*(无机化学学报), **2016**, **32**:1831-1838